IEEE Access
Multidisciplinary | Rapid Review | Open Access Journal

Received November 22, 2020, accepted December 23, 2020, date of publication December 31, 2020,
date of current version January 20, 2021.

Digital Object Identifier 10.1109/ACCESS.2020.3048354

A High Step-up Integrated Coupled Inductor-Capacitor DC-DC Converter

RAHEEL AFZAL[1,2], YU TANG[1,2], (Senior Member, IEEE), HAISHENG TONG[1,2], AND YINGJUN GUO[3]

[1]State Key Laboratory of Reliability and Intelligence of Electrical Equipment, Hebei University of Technology, Tianjin 300130, China
[2]Hebei Key Laboratory of Electromagnetic Field and Electrical Apparatus Reliability, Hebei University of Technology, Tianjin 300401, China
[3]Department of Electrical Engineering, Hebei University of Science and Technology, Shijiazhuang 050018, China

Corresponding author: Yu Tang (ty8025@hotmail.com)

This work was supported in part by the National Natural Science Foundation of China under Grant 51677084, in part by the Hebei Province Science Fund for Distinguished Young Scholars under Grant E2020202140, in part by the Support Program (III) for 100 Outstanding Innovative Talents in Universities of Hebei Province under Grant SLRC2019025, and in part by the Science and Technology Support Project of Hebei Province under Grant 20314501D and Grant 19214501D.

ABSTRACT A high step-up integrated coupled inductor-capacitor DC-DC converter for renewable energy applications has been proposed in this paper. Because of relative low output voltage of renewable energy systems, a high step-up converter is necessary. In this paper, a new configuration has been given by integrating coupled inductor-capacitor to get the desire voltage gain. The voltage gain dramatically boosted up by using a coupled inductor to charge a capacitor and the voltage across the switch are clamped inherently. The proposed converter possesses of only six components, which makes it uncomplicated and more efficient. The derivation of the steady state operation's principles has been analyzed in detail, this paper. Prototype hardware is implemented in the laboratory and the experimental results are given to verify the theoretical analysis.

INDEX TERMS Coupled inductor, high step-up converters, switch capacitor, transformer less converters.

I. INTRODUCTION

From last decade the demand of the energy across the world inclined dramatically, consequently the reserves of the fossil fuel such as oil, natural gas and coal are declining. Therefore, traditional energy sources are inadequate to meet with growing demand of the energy. Furthermore, these sources are non-renewable and emissions from these traditional energy sources are hazardous for our environment and their negative impact on the environment is irreversible [1]. Hence, it is imperative to develop new clean, renewable energy resources-based solution, such as solar energy [2]–[6]. To meet the high input voltage level of inverter, one way is to adopt series-stacking PV modules, but by using this method owing to the partial shading or module mismatch the PV system's overall output power would be declined [7]. Another solution of this problem is to boost the output of the renewable energy source by using high step-up DC-DC converter. But high voltage gain may not be achieved by using conventional boost converter or if they are operated at extreme duty cycle to achieve high voltage gain, and then because of high voltage and current stresses the overall efficiency of the converter is compromised. The voltage gain of the isolated converters can also be enlarged by enlarging the transformer's turns ratio. While the inversion and rectifying stage induces multi-stage power conversion and deduce the efficiency [8], [9]. In [10] and [11] a new technique called voltage lift is proposed. A high voltage gain is achieved by transferring energy from the intermediate capacitor but current and voltage stresses on the intermediate capacitors are high. By adjusting coupled inductor's turns ratio, the coupled inductor technique is being used in combination of various types of the converters to achieve higher voltage gain [9]–[19]. However, a high spike on the switches can be seen when the switches of the converter are turned off because of the leakage inductance of the coupled inductor. An additional passive or active voltage clamping can be used to suppress the spike of the voltage and dissipate the energy of the leaked inductance [19], [20], but these solutions would increase the hardware design difficulty and raise the system overall cost.

A high step-up integrated coupled inductor-capacitor (ICIC) converter with minimized power elements is proposed in this paper. By adopting coupled inductor and voltage lift techniques, the voltage gain of the ICIC converter has

The associate editor coordinating the review of this manuscript and approving it for publication was Ahmed Aboushady.

been enlarged. At the same time, it has some advantages like high efficiency, less components and simple structure. The proposed converter also inherits voltage clamping of power switch as boost converter. Therefore, no voltage clamping and snubber are required. The operational analysis under different working modes have been discussed and a prototype has been established in the lab. The simulation and experimental results are given to verify the analysis.

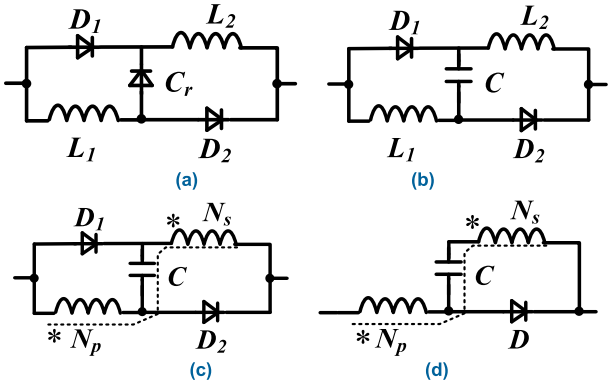

FIGURE 1. Derivation of boost unit of proposed topology (a) Switched Inductor (b) Switched inductor- Switched Capacitor Unit (c) Coupled Inductor-Switch Capacitor (d) Integrated Coupled-Inductor-capacitor (ICIC) boost unit.

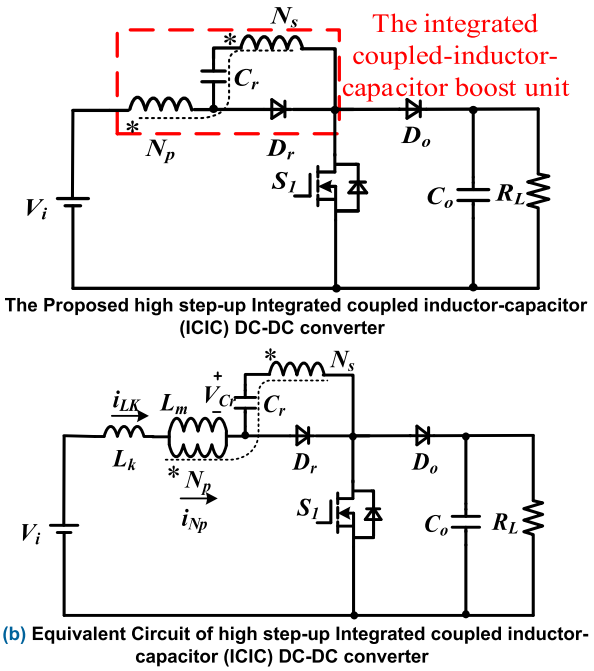

FIGURE 2. A high step-up Integrated coupled inductor-capacitor (ICIC) DC-DC converter and its equivalent circuit.

II. DERIVATION AND PRINCIPLE ANALYSIS OF ICIC CONVERTER

The proposed converter is derived from switched inductor topology as shown in figure 1. Figure 1(a) shows a switched inductor, it has low voltage gain so it is modified and a switched capacitor is inserted in it as shown in Figure 1(b). Higher voltage gain can be achieved by modifying the coupled inductor's turns ratio N_s/N_p. Therefore, a coupled inductor replaces inductors L_1 and L_2 as shown in the Figure 1(c). If the turns ratio of the coupled inductor is more than 1, then diode D_1 always remains off therefore can be removed to get ICIC boost unit as shown in Figure 1(d). The conventional boost converter's inductor can be replaced with the derived unit. The Figure 2 shows ICIC converter. The switching unit of the converter is improved and optimized, a single switch without complex control is used to operate the converter. By the combination of ICIC boost unit with the boost converter, a new converter with the coupled inductor capacitor is formed. One diodes D_r and a capacitor C_r form the typical voltage lift network. Capacitor C_r reaps energy from secondary winding N_s and also from the input source V_i and then through rectifier diode D_o delivers this energy to the output. The converter proposed in this paper has some advantages. First, the proposed converter's voltage gain is higher because of the fact that capacitor C_r gets charged from the input voltage V_i and also by the secondary winding N_s. Second, the coupled inductor will transfer the energy either the active switch S_1 is turned off or on, thus usage of coupled inductor has been increased. Third, the inrush current of the capacitor C_r gets reduced, as the coupled inductor's leakage inductance restricts the capacitor's charging current. The most important feature of proposed converter is the less part count.

A. CCM OPERATIONAL PRINCIPLE

The Figure 4 shows the key waveforms of the ICIC converter in CCM mode. Five modes have been discussed in CCM operation.

1) MODE 1 [$T_0 \sim T_1$]

The active switch S_1 is turned ON, diode D_r is in conducting state and D_0 is reverse biased during this mode as shown in the Figure 3(a). Magnetizing inductor L_m and leakage inductance L_k store energy from the input voltage source V_i. In this mode the couple inductor not only stores energy but also charges capacitor C_r. When the $t = t_1$ this mode gets ended and switch S_1 turns off.

2) MODE 2 [$T_1 \sim T_2$]

The active switch S_1 is turned off, output diode D_0 is turned on, freewheeling diode D_r is still in conducting state during this mode, as output diode is turned on so the voltage on the switch S_1 is clamped to the output capacitor, the Figure 3(b) shows the equivalent circuit. The leakage inductance current i_{LK} and magnetizing current i_{Lm} start to decline, magnetizing inductance L_m is discharged to the load and to the output capacitor C_0. When the secondary current i_{Ns} moderately decline to zero, this mode gets ended.

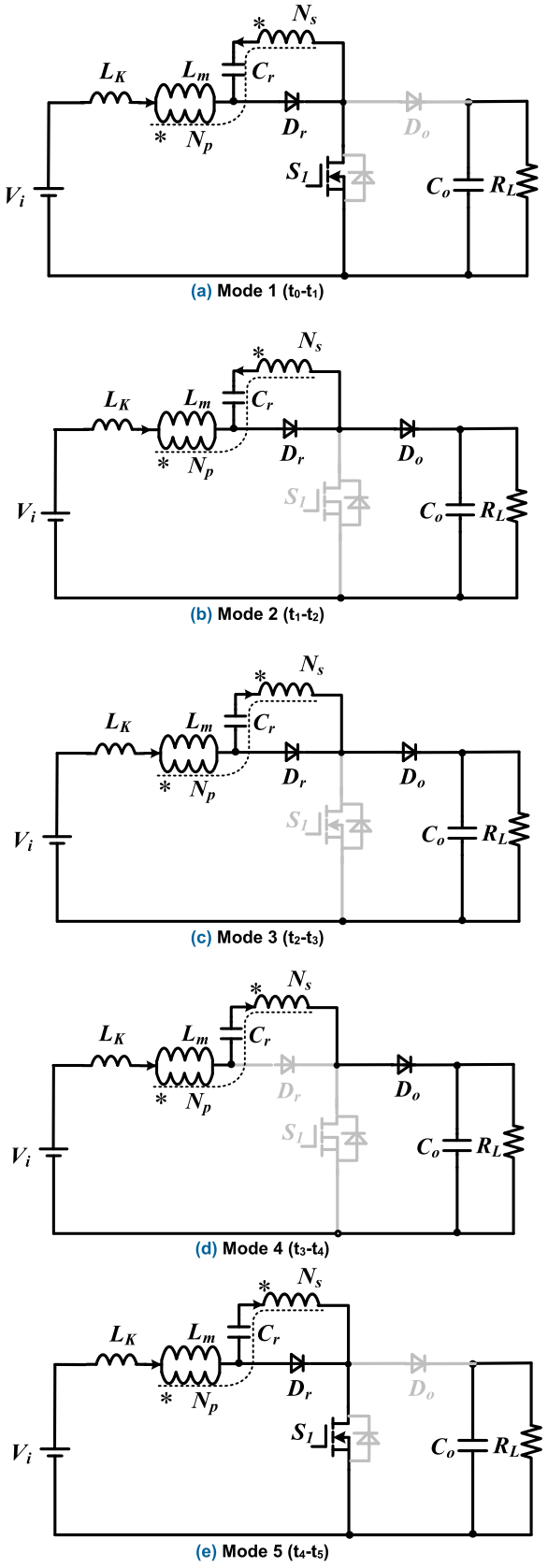

FIGURE 3. The equivalent circuit of high step up ICIC DC-DC Converter.

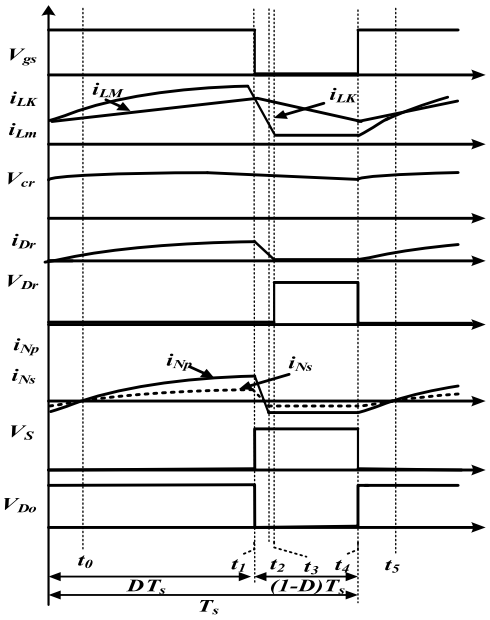

FIGURE 4. The main waveforms of CCM operation.

3) MODE 3 [$T_2 \sim T_3$]

The equivalent circuit of this mode has been shown in Figure 3(c). The output diode D_0 and freewheeling diode D_r are still in conducting stage. The secondary side and primary side currents I_{Ns}, I_{Np} increase in reverse, the leakage inductance current i_{LK} and magnetizing current i_{LM} continue to decline and energy storing capacitor C_r begins to discharge. When the freewheeling diode D_r is turned off, this mode gets ended.

4) MODE 4 [$T_3 \sim T_4$]

The equivalent circuit of this mode has been shown in Figure 3(d). The output diode D_0 is still in conducting state while the freewheeling diode D_r is turned off. The primary and the secondary sides of the coupled inductor are connected in series with the energy storage capacitor C_r and get discharged to it. The coupled inductor acts like a big inductor, the discharge current is approximately constant and equal to $i_{Lm}/(N+1)$.

5) MODE 5 [$T_4 \sim T_5$]

The Figure 3(e) shows the equivalent circuit of this mode. During this mode the output diode D_0 is turned off. The switch S_1 and freewheeling diode D_r are turned on. The input voltage source V_i charges the magnetizing inductance and the magnetizing current enlarges gradually. The energy storage capacitor C_r and the leakage inductance L_k resonate to charge the couple inductor. This mode gets ended when the coupled inductor's current of the primary and secondary sides decline to zero in reverse.

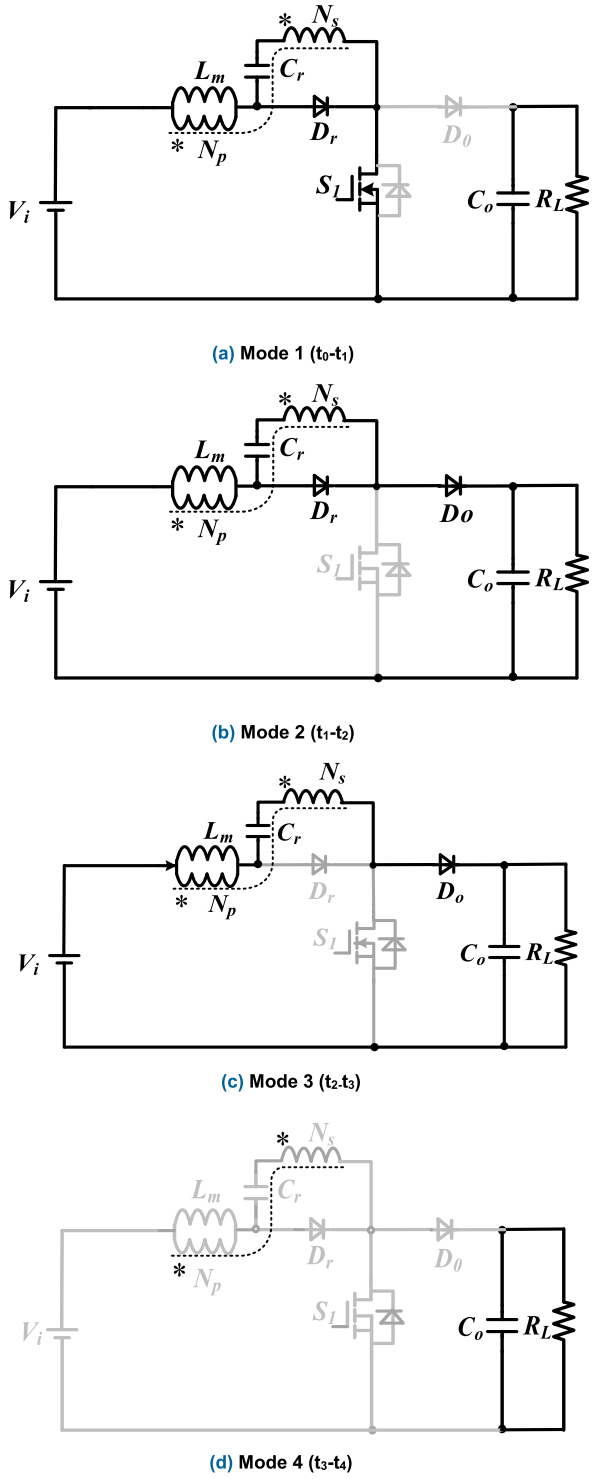

FIGURE 5. DCM modes of operation.

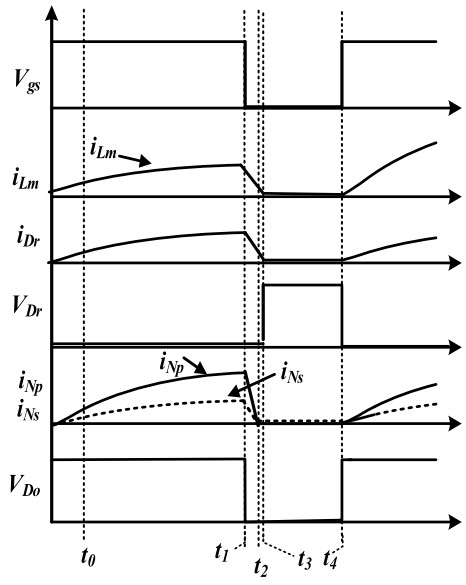

FIGURE 6. DCM Waveforms.

B. DISCONTINOUS CONDUCTION MODE OPERATIONAL PRINCIPLE

The key waveforms of the proposed converter in DCM mode has been shown in Figure 6. Four modes are being discussed in DCM operation.

1) MODE 1 [T_0-T_1]

As shown in the Figure 5(a) during the mode 1, switch S_1 is turned ON, diode D_r is in conducting state and D_0 is reverse biased. Magnetizing inductor L_m stores energy from the input voltage source V_i, coupled inductor charges the Capacitor C_r. When switch S_1 is turned off then this mode gets ended.

2) MODE 2 [T_1-T_2]

The switch S_1 is turned off, the output diode D_0 is turned on and freewheeling diode D_r is still in conducting state during this mode, as shown in Figure 5(b). The Magnetizing current i_{Lm} starts to decline, magnetizing inductance L_m is discharged to the output energy storage capacitor C_0 and to the load. This mode gets ended, when freewheeling diode is turned off.

3) MODE 3 [T_2-T_3]

The Figure 5(c) shows the equivalent circuit of this mode. The output diode D_0 is on and freewheeling diode D_r is turned off. Primary and secondary sides of coupled inductor are connected in series with the output capacitor C_O so it will charge the output capacitor.

4) MODE 4 [T_3-T_4]

The Figure 5(d) shows the equivalent circuit of this mode. During this mode the switch S_1, freewheeling diode D_r and output diode are turned off. The coupled inductor is fully discharged and output capacitor will discharge to load R_L.

C. STEADY STATE ANALYSIS OF PROPOSED CONVERTER

The absence of the complex network makes the control of the proposed converter very simple and easy to handle. In this session continuous conduction mode (CCM), Discontinues

Conduction mode (DCM) and Boundary conduction mode (BCM) are being discussed. Capacitance of the switch and parasitic resistance are ignored. The following parameters are being considered.

- All components are considered as ideal.
- The Capacitors C_r and C_0 are large enough that they have constant voltage on them.
- The coupled inductor's turns ratio is equal to N_s/N_p.
- On the primary side of the coupled inductor, the magnetizing inductance has been integrated.

The Figures 4 and 6 show the continuous conduction mode (CCM) and discontinuous conduction mode (DCM) operation typical waveforms of several key components. V_{gs} shows the gate signal of the switch S_1.

1) CCM OPERATION

By applying the voltage second balance principle on the primary side of the couple inductor N_p.

$$V_p = \frac{kD}{1-D} V_i \tag{1}$$

where k is coupling coefficient, similarly, the voltage on coupled inductor's secondary side N_s is:

$$V_s = \frac{kD}{1-D} NV_i \tag{2}$$

The voltage on the capacitor C_r is:

$$V_{Cr} = k.NV_{in} \tag{3}$$

where N is the turns ratio

The output voltage is the sum of input voltage V_i, capacitor C_r and primary N_p and secondary N_s sides of the coupled inductor. The voltage conversion ratio of CCM mode is derived as:

$$M_{CCM} = \frac{V_O}{V_i} = \frac{1 + Nk - D(1-k)}{1-D} \tag{4}$$

$$M_{CCM} = \frac{V_O}{V_i} = \frac{1 + Nk - D(1-k)}{1-D} \tag{5}$$

If the impact of leak inductance is ignored i.e K = 1 then the voltage gain of proposed converter can be expressed as:

$$M_{CCM} = \frac{V_O}{V_i} = \frac{1+N}{1-D} \tag{6}$$

Figure 7 shows the effect of various value of K on the voltage gain of the proposed converter. Figure 8 shows the relationship of gain, turns ratio and duty cycle of ICIC converter. It can be seen that by enlarging coupled inductor's turns ratio, the voltage gain of the proposed converter also increases. By selecting a modest coupled inductor's turns ratio, converter's voltage gain can be enlarged. The voltage gain of the boost converter and the proposed converter is same when N = 0. While with the increase of the N, the gain increases, which avoids the occurrence of the maximum duty cycle in boost situation.

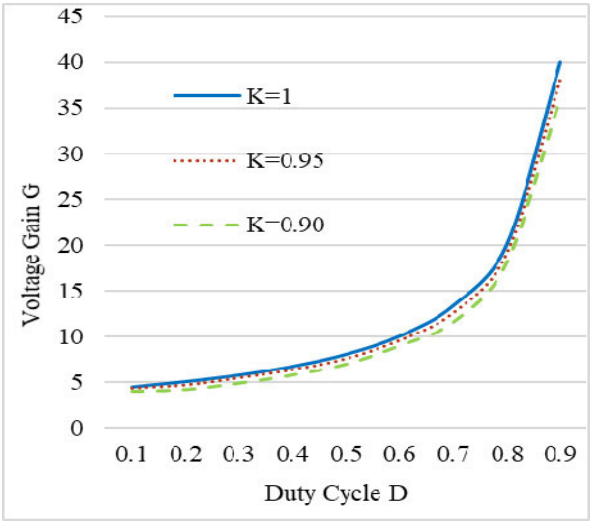

FIGURE 7. Voltage gain of proposed converter at various value of K at N = 3.

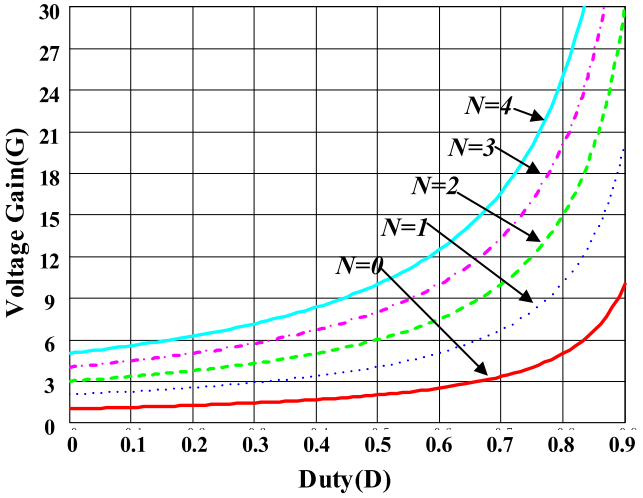

FIGURE 8. The relationship of gain, turns ratio and duty cycle of high step-up ICIC DC-DC Converter.

2) DCM OPERATION

As shown in Figure 5(a) during the mode 1, the switch of the converter is turned on. Therefore, the following equations are derived

$$V_P = V_i \tag{7}$$

$$V_s = NV_i \tag{8}$$

The value of peak magnetizing inductor current I_{Lmp} is

$$I_{Lmp} = \frac{V_i}{L_m} DT_s \tag{9}$$

Voltage across capacitor C_r is:

$$V_{Cr} = V_s = NV_i \tag{10}$$

As shown in the Figures 5(b) and 5(c), during the time interval of mode 2 and mode 3, the switch is turned off,

In the mode 2, freewheeling diode and the output diode are in conducting stage while in the mode 3 the freewheeling diode is turned off. The following equations can be derived from these modes.

$$V_{Cr} = NV_i \tag{11}$$

$$V_i = V_p + V_s + V_0 - NV_i \tag{12}$$

$$V_p = V_i - \frac{V_0}{N+1} \tag{13}$$

During the time interval of mode 4 as shown in the Figure 5(d) following equations are derived.

$$V_p = V_s = 0 \tag{14}$$

The following equations are formed, by implementing the principle of voltage second balance on N_s, N_p sides of a coupled inductor.

$$\int_0^{DTs} V_p dt + \int_{DTs}^{(D+D_L)Ts} V_p dt + \int_{(D+D_L)Ts}^{Ts} V_p dt = 0 \tag{15}$$

$$\int_0^{DTs} V_s dt + \int_{DTs}^{(D+D_L)Ts} V_s dt + \int_{(D+D_L)Ts}^{Ts} V_s dt = 0 \tag{16}$$

By using equation (15), (16) and (12)

$$D_L = \frac{(N+1)DV_i}{(N+1)V_i - V_0} \tag{17}$$

The average current I_{CO} is found as:

$$I_{C0} = I_{D0} - I_0 = 0 \tag{18}$$

$$I_{D0} = \frac{1}{2}\frac{V_i}{L_m} D_L T_s = I_0 = \frac{V_0}{R} \tag{19}$$

$$D_L = \frac{2L_m V_0}{DT_s RV_i} \tag{20}$$

From equation (20) and (17)

$$(N+1)DV_i DT_s RV_i = 2L_m V_0((N+1)V_i - V_0) \tag{21}$$

By simplifying and applying the quadratic formula, we get the DCM voltage gain as

$$M_{DCM} = \frac{1}{2}\left[(N+1) + \sqrt{(N+1)^2 + \frac{2D^2(N+1)}{\Gamma_{Lm}}}\right] \tag{22}$$

where

$$\Gamma_{Lm} = \frac{L_m}{RT_s} = \frac{L_m f_s}{R} \tag{23}$$

Figure 9 shows the values of Voltage gain during DCM operation at various value of Γ_{Lm}.

3) BOUNDARY CONDUCTION MODE (BCM) OPERATION

When the proposed convert is being operated in the boundary conduction mode (BCM), the voltage gain of both continuous conduction mode (CCM) and discontinuous conduction mode (DCM) operations are equal to each other.

So, from the (6) and (22), the magnetic boundary is:

$$L_m = \frac{2D^2(1-D)^2 R}{(N+1)[(1+D)^2 - (1-D)^2]f_s} \tag{24}$$

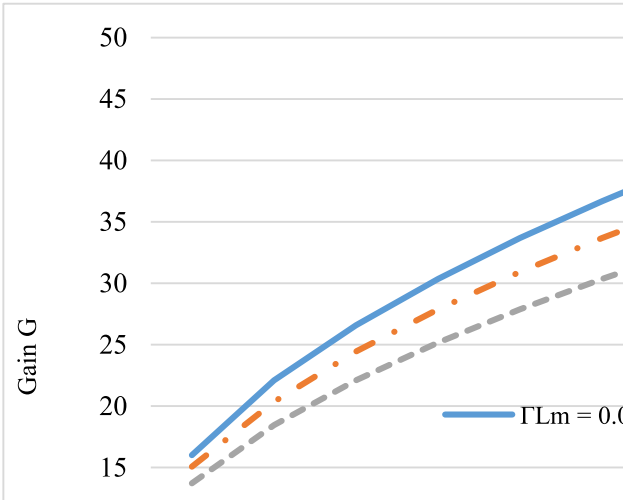

FIGURE 9. During DCM operation Voltage gain against duty ratio at different values of Γ_{Lm}.

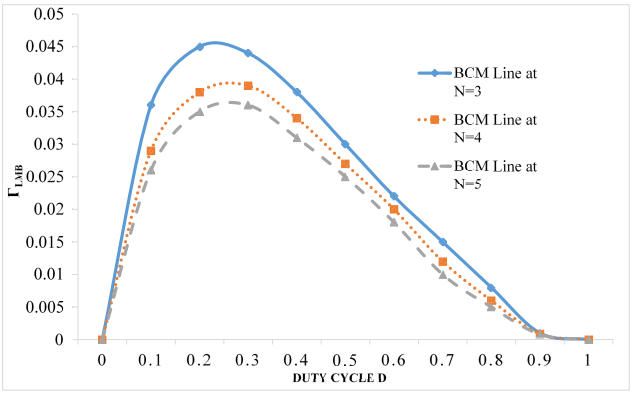

FIGURE 10. BCM of High step-up ICIC DC-DC Converter at various turns ratio.

The BCM of ICIC converter at various turns ratio is shown in Figure 10. The proposed converter will operate in the CCM, if the value of Γ_{Lm} is larger than Γ_{LmB}.

III. VOLTAGE AND CURRENT STRESSES ON DEVICES

By using equation (3) the voltage stress on the capacitor C_r is:

$$V_{C_r} = NV_i \tag{25}$$

Voltage stress on freewheeling diode D_r can be expressed as:

$$V_{D_r} = \frac{1}{1-D} NV_i \tag{26}$$

Voltage on the output diode is equal to the output voltage.

$$V_{D_O} = V_O \tag{27}$$

The average on-state currents of secondary side of couple inductor I_s and output diode D_o are expressed as

$$I_{D0} = I_0 \tag{28}$$

$$I_s = \frac{NI_O}{1-D} \tag{29}$$

According to the flux balance equation.

$$N_p I_p = (N_p + N_s) I_s \tag{30}$$

By using equation (29) and (30), the average on-state current of primary side of couple inductor I_p and switch I_{Switch} can be derived as:

$$I_{Switch} = I_p = \frac{N(N+1)I_O}{1-D} \tag{31}$$

Similarly, the on-state current of freewheeling diode is:

$$I_{Dr} = \frac{NI_O(N+2)}{1-D} \tag{32}$$

IV. PARAMETERS DESIGN

To find the value of the capacitor C_r following equation can be used.

$$C_r \geq \frac{I_O}{\Delta V_{c_r} f_S} = \frac{P_O}{\Delta V_{c_r} f_S V_O} \tag{33}$$

where the output power of the converter is PO. ΔV_{cr} is the percentage of ripples

Similarly, value of output capacitor can be derived as follows:

$$C_O \geq \frac{DI_O}{\Delta V_{C_O} f_S} \tag{34}$$

I_O is the output current and ΔV_O is the percentage of ripples in the output voltage.

The coupled inductor's turns ratio can be found by using following equation

$$N = \frac{V_O}{V_i}(1-D) - 1 \tag{35}$$

By using equation (24) the minimum value of Magnetizing inductance L_{min} can be calculated.

The magnetizing inductance value of designed coupled inductor should be more than L_{min}.

V. PERFORMANCE COMPARISON

In this section, the proposed converter is compared with four other converters. Table 1 and Figure 1 show the comparison of ICIC converter with the converters in [21]–[24]. It can be seen that the proposed converter shows better performance than other converters in terms of voltage gain and number of components being used. The ICIC converter is simple and only have one switch like traditional Boost converter, by using the topology of coupled inductor-capacitor, the proposed converter can achieve high voltage gain with small duty cycle, which makes it much more efficient than the converters discussed in [21]–[24].

VI. POWER LOSS DISTRIBUTION

In this section, the power loss of the proposed converter is evaluated in order to verify converter performance. The proposed converter operates under the condition given in Table 1.

$$P_{Sw} = 0.5 f_s V_s I_s (t_{off} + t_{on}) \tag{36}$$

TABLE 1. Comparison of ICIC Converter with converter in [21]–[24].

	Proposed converter	[21]	[22]	[23]	[24]
Voltage gain	$\frac{N+1}{1-D}$	$N+\frac{2-D}{1-D}$	$\frac{1-ND}{1-D}$	$ND+\frac{2}{1-D}$	$N+\frac{2}{1-D}$
No of components	6	9	6	11	8
Switch	1	2	1	2	2
Diodes	2	1	2	4	2
Inductor	2	3	2	2	2
Capacitor	1	3	1	3	2
$V_{stress\text{-}Switch}$	G	$G+\frac{ND-1}{1-D}$ $G-2+\frac{ND}{1-D}$	G	$\frac{G-ND}{2G}$	$G+\frac{D(N-D)}{1-D}$ $G+\frac{D(N-1)-1}{1-D}$
V_{in}-V_o/ P_o/ η(max)/ f_s	40-400V/ 250W/ 97%/ 100kHz	12-72V/ 72W/ 95%/ 100kHz	25-230V/ 150W/ 90%/ 100kHz	24-200V/ 400W/ 95.8%/ 50kHz	24-170V/ 240W/ 94.8%/ 200kHz

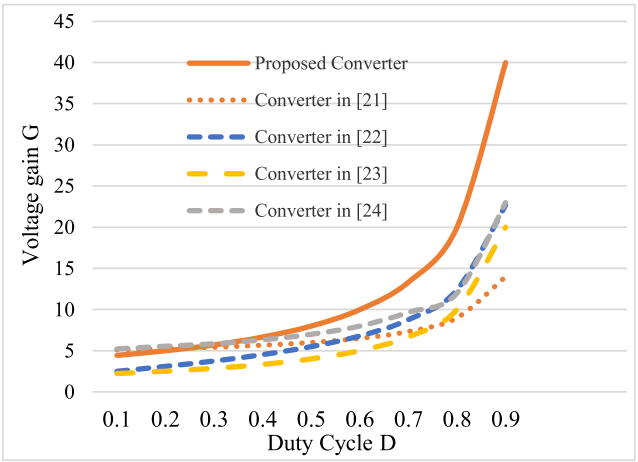

FIGURE 11. The Voltage gain Comparison of converter in [21]–[24] with high step-up ICIC DC-DC Converter at N = 3.

where f_s is the switching frequency, V_s is maximum voltage stress of the switch and I_s is the current of the switch during the switching time, t_{off} and t_{on} are given by device static characteristics provided by datasheet.

The conduction loss can be estimated as:

$$P_{Scon} = I^2_{S(rms)} R_{DS(on)} \tag{37}$$

where $I_{s(rms)}$ is the switch rms current and $R_{DS(on)}$ is the MOSFET ON-state resistance. For switch S, the losses are due to switching and conduction. The switching loss of the switch can be estimated as follows:

The total loss of the MOSFET is given by:

$$P_S = P_{Sw} + P_{Scon} \tag{38}$$

The conduction loss of the diodes can be estimated as:

$$P_D = I_{D(rms)} V_F \tag{39}$$

where $I_{D(rms)}$ is the rms current and V_F is the diode threshold voltage. V_F is considered from characteristics given by the datasheet.

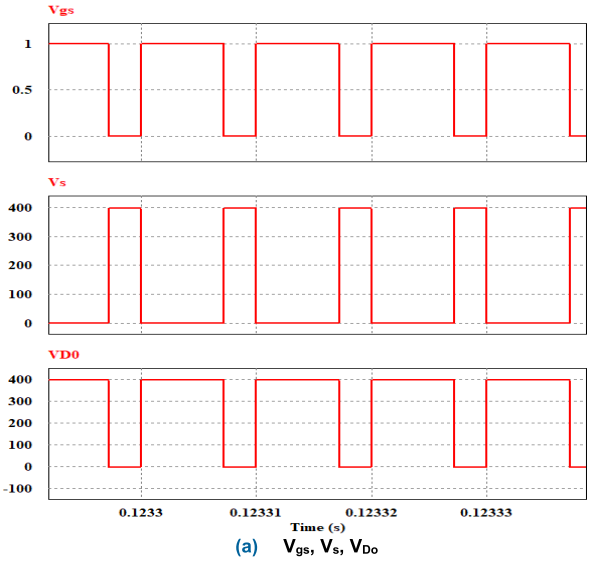

(a) V_{gs}, V_s, V_{Do}

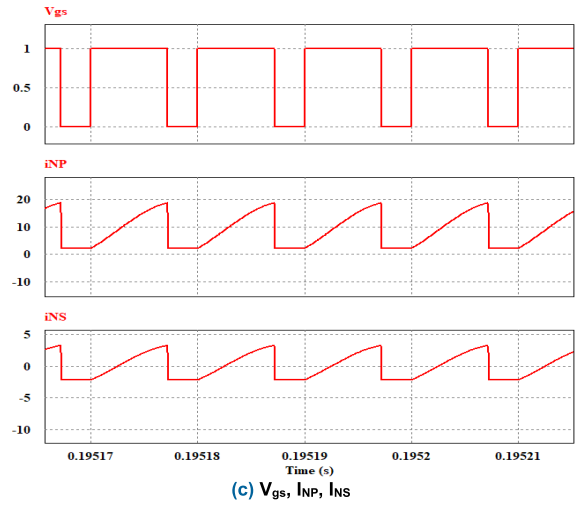

(c) V_{gs}, I_{NP}, I_{NS}

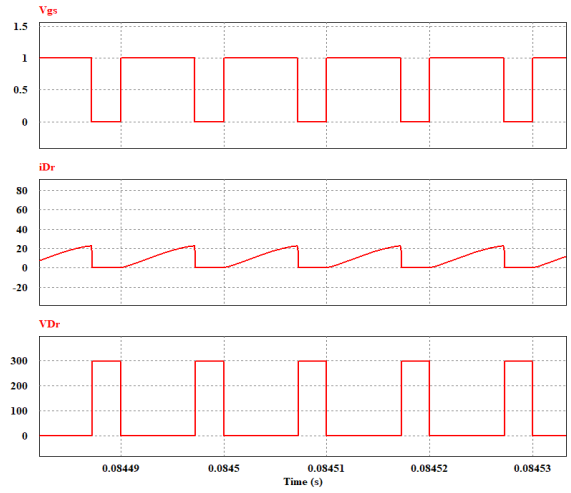

(b) V_{gs}, I_{Dr}, V_{Dr}

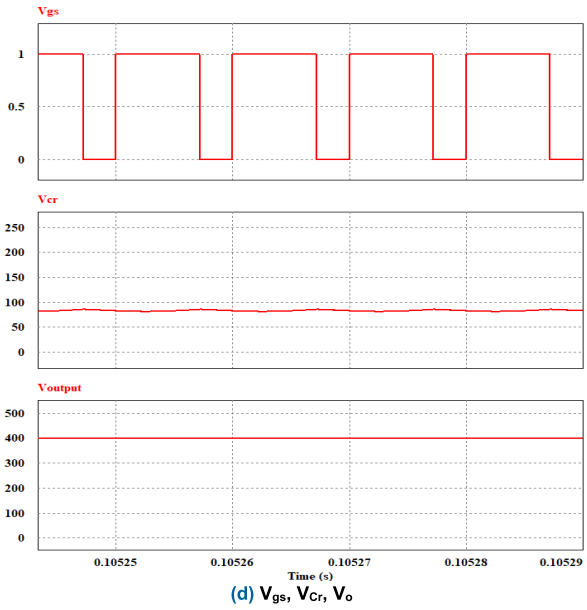

(d) V_{gs}, V_{Cr}, V_o

FIGURE 12. Simulation Results of proposed Converter.

The magnetic device losses can be estimated by:

$$P_L = r_L I_{Lrms}^2 + (aB_{pk}^b f_s^c) A_e l_e + 0.5 f_s L_k I_{Lpeak}^2 \quad (40)$$

where $I_{L(rms)}$ is the rms current of the couple inductor; B_{pk} is the ac magnetic flux density for the magnetic device core; l_e is the core medium path length, A_e is the transversal core area, a, b, and c are constants determined from curve fitting of the core.

So, capacitor losses can be calculated as:

$$P_C = \sum_{g=1}^{G} I_{Crms}(g)^2 ESR_{(g)} \quad (41)$$

where I_{Crms} is the rms current and ESR is the measured resistance of the capacitor.

VII. SIMULATION AND EXPERIMENTAL RESULTS AND DISCUSSION

The ICIC Converter is designed and analyzed. At input voltage 30V, switching frequency 100 kHz, thekey waveforms, voltage stress on the power devices and voltage gain are analyzed and results are compared with the theoretical results. Figure 11 shows the results of simulation in the PSIM.

V_{gs} shows the voltage across the gate terminal of the MOSFET, I_{Dr}, V_{Dr} shows the current and voltage across the freewheeling diode D_r respectively. V_{Do} is the voltage across the output diode and V_{Cr} is the voltage across the capacitor Cr. i_{Np} and i_{Ns} are the currents in the primary and secondary windings of the coupled inductor. Figure 12 (a) shows the voltage stress across the output diode D_o, it can be seen that voltage across output diode D_o is equal to theoretical calculated voltage by using equation (27). Figure 12 (b) shows the

TABLE 2. System specifications.

System parameters	Specifications
Input Voltage V_i	20V- 40V
Output Voltage V_o	400V
Output Power P_o	250W
Switching Frequency f_s	100kHz
Power Switch S	IRFP460/ IPW50R140CP
Diode D_r	MUR1540
Diode D_o	IDH06G65C5
Turns Ration of Coupled Inductor	$N_P : N_S$=1:3
Capacitor C_r	2.2uF/250V
Capacitor C_o	470uF/450V

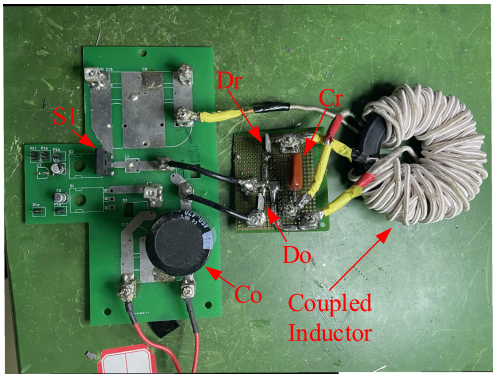

FIGURE 13. Prototype of proposed converter.

current and voltage stresses across freewheeling diode D_r, it can be seen that theoretical calculations of freewheeling diod's current and voltage stress by using equation (32) and (26) coincide with the results of figure 12 (b). Figure 12 (c) shows the current in the coupled inductor's primary i_{Np} and secondary i_{N}s windings, the value of current i_{Np} and i_{N}s in the winding consistent with the theoretical values calculated by using equations (29) and (31) respectively. It can be observed that both primary and secondary winding are connected in series when switch S is turned off. Figure 12 (d) shows output voltage V_o and the voltage across the capacitor C_r. The theoretical output voltage V_o calculated by using equation (6) is equal to the simulation value and theoretical calculation of voltage across capacitor C_r by using equation (25) is equal to the results as shown in Fig. 12 (d).

A 250 W prototype is designed and analyzed to verify the theoretical and simulation results of proposed converter. Table 2 shows the system specifications of the proposed converter and Figure 13 shows the prototype hardware established in the laboratory.

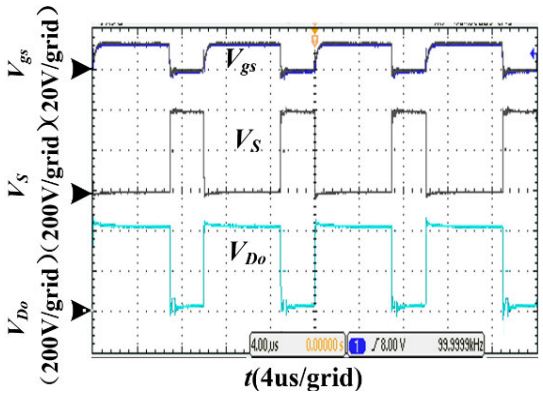

FIGURE 14. Voltage of the gate signal V_{gs}, voltage across the switch V_S and voltage across the output diode V_{DO}.

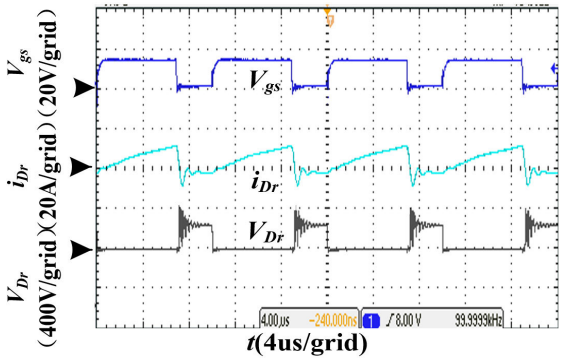

FIGURE 15. Voltage of the gate signal V_{gs}, voltage V_{Dr} and current I_{Dr} of the freewheeling diode D_r.

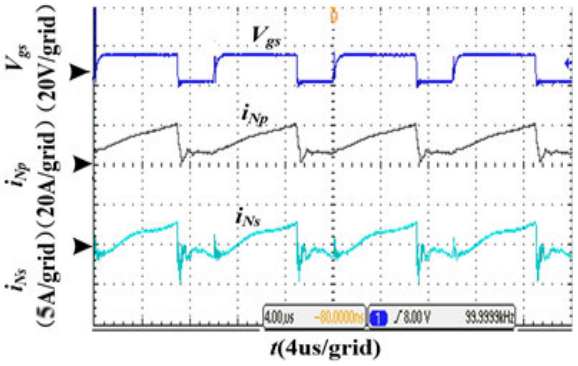

FIGURE 16. Voltage of the gate signal V_{gs}, coupled inductor's primary and secondary sides current I_{NP}, I_{NS}.

Figures 14-16 illustrate the experimental waveforms of the proposed converter. With the input voltage of 30V the output is 400V and 250W. Figure 14 shows the voltage of the gate signal V_{gs}, voltage across the switch S1 and voltage across the output diode D_0.

It can be seen that the voltage stress on the active switch S_1 is equal to the output voltage i.e.400V. Figure 15 shows the waveform voltage V_{Dr} and current I_{Dr} of the freewheeling diode D_r. The voltage stress on the freewheeling diode is

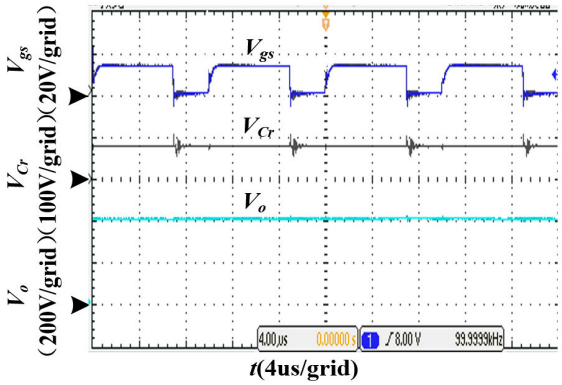

FIGURE 17. Voltage of the gate signal V_{gs}, voltage of the capacitor V_{Cr} and output voltage V_O.

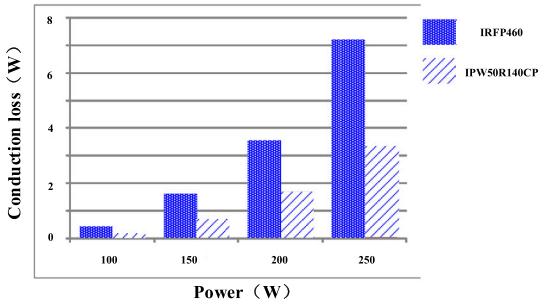

FIGURE 18. Comparison of conduction loss.

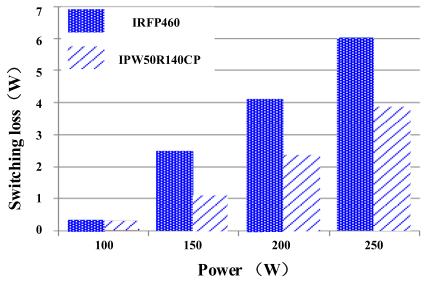

FIGURE 19. Comparison of switching loss.

300V which proves the theoretical calculation of the voltage stress on it, under the effect of leakage inductance the current of freewheeling diode i_{Dr} declines and as a result the voltage across the diode D_r rises.

Figure 16 shows the current waveforms of the primary and secondary winding of the coupled inductor. It can be seen that primary and secondary windings are connected in series, when the switch is turned off.

Figure 17 shows the voltage waveform of the capacitor C_r and output voltage. The voltage waveform of V_{Cr} remains constant because of the large capacitance value.

The COOLMOS (IPW50R140CP) and MOSFET IRFP460 is used as power switch and the power losses of the two kinds of power switches in the proposed converter are compared. For power devices of the same voltage and current level,

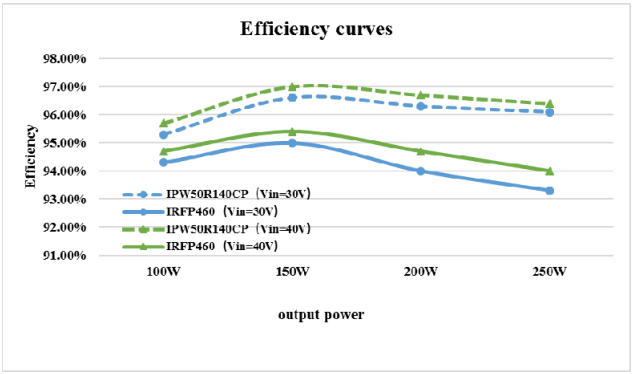

FIGURE 20. Comparison of efficiency curves with different switches.

COOLMOS has better performance in terms of the conduction power losses and switching power losses. As shown in Figures 18&19, under 40V input voltage, the conduction and switching power losses of switch are reduced with IPW50R140CP, which is more suitable for the application of ICIC converter.

VIII. CONCLUSION

Based on the switching unit, this paper presents a ICIC converter, by extracting the coupled-inductor-capacitor boost unit and integrating it with Boost converter, the voltage gain can reach higher easily by changing the turn ratio of the coupled inductor. The proposed converter possesses of only six components, which makes it uncomplicated and more efficient. And finally, this paper verifies the precision of the proposed converter through simulations and hardware testing. A prototype hardware of High step-up ICIC DC-DC converter is designed and tested in the laboratory, which gives highest efficiency 97%.

REFERENCES

[1] K.-C. Tseng, C.-C. Huang, and W.-Y. Shih, "A high step-up converter with a voltage multiplier module for a photovoltaic system," *IEEE Trans. Power Electron.*, vol. 28, no. 6, pp. 3047–3057, Jun. 2013.

[2] K.-C. Tseng and C.-C. Huang, "High step-up high-efficiency interleaved converter with voltage multiplier module for renewable energy system," *IEEE Trans. Ind. Electron.*, vol. 61, no. 3, pp. 1311–1319, Mar. 2014.

[3] JV. Karthikeyan and R. Gupta, "Multiple-input configuration of isolated bidirectional DC–DC converter for power flow control in combinational battery storage," *IEEE Trans. Ind. Informat.*, vol. 14, no. 1, pp. 2–11, Jan. 2018.

[4] S. Ding, W. X. Zheng, J. Sun, and J. Wang, "Second-order sliding-mode controller design and its implementation for buck converters," *IEEE Trans. Ind. Informat.*, vol. 14, no. 5, pp. 1990–2000, May 2018.

[5] F. Li and H. Liu, "A cascaded coupled inductor-reverse high step-up converter integrating three-winding coupled inductor and diode–capacitor technique," *IEEE Trans. Ind. Informat.*, vol. 13, no. 3, pp. 1121–1130, Jun. 2017.

[6] S.-M. Chen, T.-J. Liang, L.-S. Yang, and J.-F. Chen, "A boost converter with capacitor multiplier and coupled inductor for AC module applications," *IEEE Trans. Ind. Electron.*, vol. 60, no. 4, pp. 1503–1511, Apr. 2013.

[7] R. T. Bambang, A. S. Rohman, C. J. Dronkers, R. Ortega, and A. Sasongko, "Energy management of fuel cell/battery/supercapacitor hybrid power sources using model predictive control," *IEEE Trans. Ind. Informat.*, vol. 10, no. 4, pp. 1992–2002, Nov. 2014.

[8] D. Meneses, F. Blaabjerg, Ó. García, and J. A. Cobos, "Review and comparison of step-up transformerless topologies for photovoltaic AC-module application," *IEEE Trans. Power Electron.*, vol. 28, no. 6, pp. 2649–2663, Jun. 2013.
[9] J. Lee, T. Liang, and J. Chen, "Isolated coupled-inductor-integrated DC–DC converter with nondissipative snubber for solar energy applications," *IEEE Trans. Ind. Electron.*, vol. 61, no. 7, pp. 3337–3348, Jul. 2014.
[10] Q. Zhao and F. C. Lee, "High-efficiency, high step-up DC–DC converters," *IEEE Trans. Power Electron.*, vol. 18, no. 1, pp. 65–73, Jan. 2003.
[11] W. Li, X. Xiang, C. Li, W. Li, and X. He, "Interleaved high step-up ZVT converter with built-in transformer voltage doubler cell for distributed PV generation system," *IEEE Trans. Power Electron.*, vol. 28, no. 1, pp. 300–313, Jan. 2013.
[12] S. M. Chen, T. J. Liang, L. S. Yang, and J. F. Chen, "A cascaded high step-up DC–DC converter with single switch for microsource applications," *IEEE Trans. Power Electron.*, vol. 26, no. 4, pp. 1146–1153, Apr. 2011.
[13] S. K. Changchien, T. J. Liang, J. F. Chen, and L. S. Yang, "Novel high step-up DC–DC converter for fuel cell energy conversion system," *IEEE Trans. Ind. Electron.*, vol. 57, no. 6, pp. 2007–2017, Jun. 2010.
[14] S. Zhang, J. Xu, and P. Yang, "A single-switch high gain quadratic boost converter based on voltage-lift-technique," in *Proc. 10th Int. Power Energy Conf. (IPEC)*, Nov. 2012, pp. 71–75.
[15] F. L. Luo, "Seven self-lift DC–DC converters, voltage lift technique," *IEE Proc.-Electr. Power Appl.*, vol. 148, no. 4, pp. 329–338, Jul. 2001.
[16] K. I. Hwu and Y. T. Yau, "High step-up converter based on coupling inductor and bootstrap capacitors with active clamping," *IEEE Trans. Power Electron.*, vol. 29, no. 6, pp. 2655–2660, Jun. 2014.
[17] X. Hu and C. Gong, "A high voltage gain DC–DC converter integrating coupled-inductor and diode–capacitor techniques," *IEEE Trans. Power Electron.*, vol. 29, no. 2, pp. 789–800, Feb. 2014.
[18] Y.-P. Hsieh, J.-F. Chen, L.-S. Yang, C.-Y. Wu, and W.-S. Liu, "High-conversion-ratio bidirectional DC–DC converter with coupled inductor," *IEEE Trans. Ind. Electron.*, vol. 61, no. 1, pp. 210–222, Jan. 2014.
[19] G. Di Capua and N. Femia, "A critical investigation of coupled inductors SEPIC design issues," *IEEE Trans. Ind. Electron.*, vol. 61, no. 6, pp. 2724–2734, Jun. 2014.
[20] W. Li, X. He, C. Xu, Y. Gu, and H. Yu, "Analysis, design and implementation of isolated bidirectional converter with winding-cross-coupled inductors for high step-up and high step-down conversion system," *IET Power Electron.*, vol. 7, no. 1, pp. 67–77, Jan. 2014.
[21] K. I. Hwu and W. Z. Jiang, "Voltage gain enhancement for a step-up converter constructed by KY and buck-boost converters," *IEEE Trans. Ind. Electron.*, vol. 61, no. 4, pp. 1758–1768, Apr. 2014.
[22] Y. Berkovich and B. Axelrod, "Switched-coupled inductor cell for DC–DC converters with very large conversion ratio," *IET Power Electron.*, vol. 4, no. 3, pp. 309–315, Apr. 2011.
[23] C.-M. Lai, C.-T. Pan, and M.-C. Cheng, "High-efficiency modular high step-up interleaved boost converter for DC-microgrid applications," *IEEE Trans. Ind. Appl.*, vol. 48, no. 1, pp. 161–171, Jan. 2012.
[24] K. I. Hwu and Y. T. Yau, "Inductor-coupled KY boost converter," *Electron. Lett.*, vol. 46, no. 24, pp. 1624–1626, Nov. 2010.

RAHEEL AFZAL received the B.S. degree in electronics engineering from The Islamia University Bahawalpur (IUB), Pakistan, in 2013, and the M.S. degree in energy systems engineering from the National University of Science and Technology (NUST), Islamabad, Pakistan, in 2016. He is currently pursuing the Ph.D. degree with the School of Electrical Engineering, Hebei University of Technology Tianjin, China. His research interests include power electronics and renewable energy generation.

YU TANG (Senior Member, IEEE) received the B.S. and Ph.D. degrees in electrical engineering from the Nanjing University of Aeronautics and Astronautics (NUAA), China, in 2003 and 2008, respectively. Since 2008, he has been with the Electrical Engineering Department, NUAA. Since 2018, he has been with the State Key Laboratory of Reliability and Intelligence of Electrical Equipment, Hebei University of Technology. He has published more than 80 papers in journals and conference proceedings. His research interest includes power electronics in renewable energy generation.

HAISHENG TONG was born in Anhui, China. He received the B.S. degree in electrical engineering from the Hebei University of Technology, Tianjin, China, in 2018, where he is currently pursuing the M.S. degree. His current research interest includes power electronics in renewable energy generation.

YINGJUN GUO received the master's degree from the Beijing Institute of Technology, China, in 2004. He is currently pursuing the Ph.D. degree in control theory and control engineering with the Hebei University of Technology. He is also an Associate Professor with the Hebei University of Science and Technology. His research interests include wind power control and power electronic devices.